View Article Online
DOI: 10.1039/C9CP06015D

PCCP

ARTICLE TYPE

Cite this: DOI: 00.0000/xxxxxxxxxx

Octahedrally Coordinated Single Layer CaF_2: Robust Insulating Behaviour†

Mehmet Baskurt,*[a] Jun Kang,[b‡] and Hasan Sahin[a]

Received Date
Accepted Date

DOI: 00.0000/xxxxxxxxxx

Using first-principles calculations, structural, vibrational, and electronic properties of single-layer calcium fluoride (CaF_2) are investigated. Dynamical stability of 1T-CaF_2 is confirmed by the phonon dispersions. Raman active vibrational modes of 1T-CaF_2 enable its characterization via Raman spectroscopy. In addition, the calculated electronic properties of 1T-CaF_2 confirmed insulating behavior with an indirect wide band gap which is larger than that of well-known single-layer insulator, h-BN. Moreover, one-dimensional nanoribbons of CaF_2 are investigated for two main edge orientations, namely zigzag and armchair, and it is revealed that both structures maintain the 1T nature of CaF_2 without any structural edge reconstructions. Electronically, both types of CaF_2 nanoribbons display robust insulating behavior with respect to the nanoribbon width. Results show that both 2D and 1D form of 1T-CaF_2 show potential in nanoelectronics as an alternative to the widely-used insulator h-BN with its similar properties and wider electronic band gap.

1 Introduction

CaF_2 is a material with wide range of applications owing to its significant properties. In dentistry, CaF_2 is used as an effective agent for preventing dental decay and increasing microbial resistance.[1–4] Due to the transparency in the infrared region, CaF_2 is found in useful in infrared spectroscopy.[5–7] In addition, CaF_2 is widely used to build lasers.[8–13] With the increasing demand in new two-dimensional (2D) materials thin films have been grown by numerous methods. Thin films of CaF_2 started gaining attention in nanoelectronic applications.[14] Number of studies relating to grow ultrathin CaF_2 films are continues with increasing trend.

2D materials gained massive interest since discovery of graphene due to their distinctive properties.[15,16] Graphene, atomically thick honeycomb structure of carbon with Dirac point,[17] is studied extensively because of its semimetallicity. However, lack of band gap limits its usage in applications. Other 2D materials are examined in order to overcome this problem and find new possible materials for devices. Materials such as transition metal dichalcogens (TMDs),[18–29] Xenes (X= Si, Ge, Sn, Pb)[30–37] are found to have semiconducting or semimetallic electronic structure, used in many device applications.[38,39] Magnetic members of family of 2D materials show promising applications in spintronics.[40–43] Moreover, the advances in nanoelectronics, insulating materials in nanoscale are required.

Most of the applications in nanoscale that have been demonstrated so far, have used h-BN as an insulating layer. It is reported to have band gap of 5.765 eV.[44] It is shown to lower the work function of the covered material. Utilizing its insulating characteristic, h-BN is reported to be sandwiched between two semiconductors, MoS_2 and GaN, a new diode is fabricated.[45] A method called “patterned regrowth" is reported by Levendorf *et al.*,[46] which allows spatial control over graphene and h-BN which provides a new approach for new low dimensional electronics. Reports indicate that h-BN have significant properties other than its insulating character. One of the important properties of h-BN is its thermal stability. h-BN is reported to remain stable up to 850°C.[47] Thermal stability at high temperatures makes h-BN a beneficial material in nanodevices which tend to operate at high temperatures. In addition to that, being an inert crystal, coating a surface with h-BN prevents surface degradation.[48]

Low dimensional crystals of CaF_2 is grown epitaxially even before the discovery of graphene.[49] However, in our best knowledge, studies about 2D CaF_2 in 1T structure are limited. Ultrathin CaF_2 recently epitaxially grown on bilayer MoS_2 to be used in building a field effect transistor (FET) as it is reported by Illarionov *et al.*.[50] This FET is found to have low subthreshold swings of 90mV dec^{-1} and up to 10^7 on/off current ratios. Based on these results, CaF_2 is believed to have particular potential in 2D electronics. In this study, motivated by the potential hold by CaF_2 in nanotechnology, properties of 2D and 1D CaF_2 structures are predicted by performing *ab* initio calculations. Phonon and electronic band structures are presented for the dynamically stable CaF_2 monolayer. Results are compared with the well-known 2D

[a] *Department of Photonics, Izmir Institute of Technology, 35430, Izmir, Turkey. E-mail: mehmetbaskurt@iyte.edu.tr*
[b] *Beijing Computational Science Research Center, Beijing, 100193, China.*

View Article Online
DOI: 10.1039/C9CP06015D

insulator h-BN.

The paper is organized as follows: details of computational methodology are given in section 2. Structural, vibrational, and electronic properties of pristine CaF_2 with 1T structure are presented in section 3. Nanoribbons of CaF_2 are examined by means of width dependency in section 4. Results are concluded in section 5.

2 Computational Methodology

First-principles calculations within density functional theory (DFT) were carried out in order to determine structural, vibrational and electronic properties of monolayer CaF_2 by using Vienna *ab-initio* Simulation Package (VASP)[51,52] with the implemented plane-wave projector-augmented wave (PAW)[53] potentials. For the exchange-correlation functional, the generalized gradient approximation (GGA) of Perdew-Burke-Ernzerhof (PBE)[54] was used. The van der Waals corrections were implemented by the DFT-D2 method of Grimme.[55] The kinetic energy cutoff of the plane-wave basis set was 500 eV in all calculations. Total energy difference of 10^{-5} eV between consequent steps was taken as convergence criteria. Gaussian smearing width of 0.05 eV was set for the density of states (DOS) calculations. At least 15 Å of vacuum spacing was taken in all calculations in order to prevent any interactions between adjacent layers. Γ centered *k*-point mesh for the primitive cell with the size of 7×7×1 was used for calculating structural and vibrational properties and 13×13×1 was used for density of states (DOS) calculations. In order to increase the accuracy of electronic band calculations, Heyd-Scuseria-Ernzerhof (HSE) functional was used.[56,57] Geometric relaxation of atoms were allowed until pressures in all directions were less than 1 kB. The vibrational properties of the structure were investigated by the small displacement method that used to calculate the phonon dispersion curves as implemented in the PHON code.[58] The charge transfer analysis was carried out by effective charge difference on atoms that was obtained by Bader technique.[59]

3 Results

Truncation of the bulk, face-centered-cubic (FCC) fluorite structured CaF_2, or epitaxial growth of calcium fluorite crystal in (111) direction as a single layer leads to the formation of CaF_2 in 1T structure. Crystal structure of 1T-CaF_2, consisting of one Ca atom sandwiched between two trigonally arranged F atoms in its primitive cell, is shown in Figure 1(a). The primitive cell of the 1T-CaF_2 has a hexagonal symmetry, with the optimized lattice parameters of 3.58 Å. Bond legth between Ca and F atoms is 2.29 Å. The Bader analysis results reveal that each Ca atom in unit cell donates 1.6 *e* while each F atom receives 0.8 *e*. Cohesive energy per atom in the unit cell of single layer CaF_2 is calculated to be 5.42 eV. In comparison with other 2D materials, cohesive energy of CaF_2 is higher than MoS_2, which is reported as 5.05 eV per atom,[60] lower than graphene and h-BN, which are reported to be 10.04 eV[61] and 7.01 eV[62] per atom, respectively.

Vibrational properties of CaF_2 crystal in 1T phase are studied through their phonon dispersions. Dynamical stability is confirmed by all real eigenvalues in the phonon band diagram.

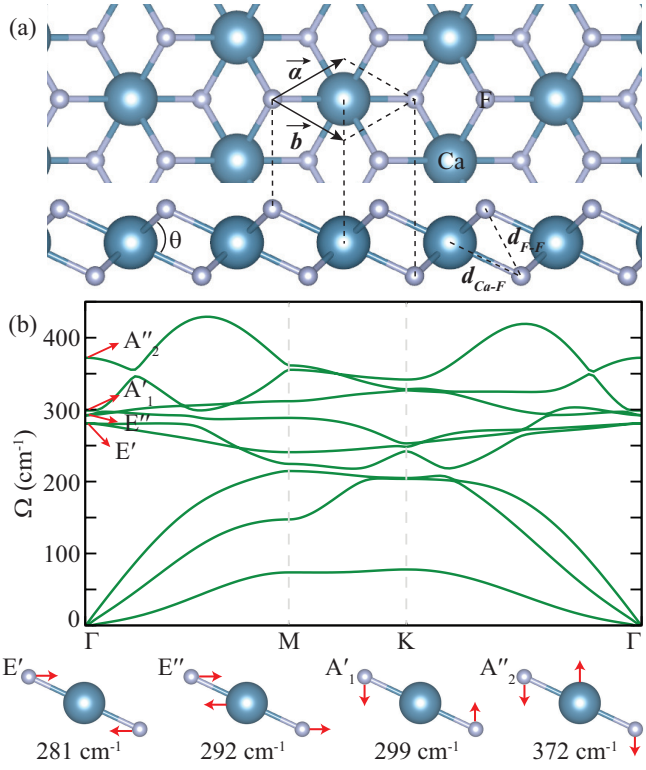

Fig. 1 (a) Top and side views of 1T-CaF_2. (b) Phonon dispersion of 1T-CaF_2. Modes with corresponding frequencies are shown in the inset.

Phonon bands and characteristics of each optical mode are presented in Figure 1(b). Unit cell of 1T-CaF_2 has one Ca and two F atoms, which displays 9 phonon modes in total; 3 acoustical and 6 optical. In optical modes there are 2 single degenerate modes, at 299 and 372 cm^1, and 2 double degenerate modes, at 281 and 292 cm^1. Due to hexagonal symmetry of the unit cell, phonon band crossing appears at K point in the Brillouin zone. Decomposition of optical modes at Γ point gives $\Gamma = 2E' + 2E'' + A'_1 + A''_2$, where E', E'', A'_1, and A''_2 are Raman active modes and have frequency of 281, 292, 299, and 372 cm^{-1}, respectively. In comparison with h-BN, the phonon bands of 1T-CaF_2 have lower frequency. Highest phonon band frequency at Γ point of h-BN is reported to be at 1345 cm^{-1}, which is 973 cm^{-1} higher than the highest phonon band frequency of CaF_2 that is observed to be at 372 cm^{-1}. This difference indicates that 1T-CaF_2 is a softer 2D structure than h-BN. In addition, mechanical properties such as in-plane stiffness and Poisson ratio are calculated as 44 N/m and 0.24, respectively. In order to determine the thermal stability of 1T-CaF_2, *ab-initio* Molecular Dynamics simulations are carried out. For the MD simulations NVE ensemble is used. K-point sampling is taken 2×2×1 for 5×5×1 supercell. The temperature is increased from 0 K to 1000 K in 10 ps with 2 fs between consequent steps. Results of the simulations reveal that CaF_2 monolayer is able to withstand such high temperatures.

Electronic band dispersions clearly indicate that 1T-CaF_2 is a wide band gap insulator as it is presented in Figure 2 (a). Band gap of the single layer CaF_2 is calculated to be 7.17 eV. major contributions to the valence and conduction bands arise from the F-*p*

View Article Online
DOI: 10.1039/C9CP06015D

Table 1 Properties of 2D CaF_2 and h-BN are as follows: lattice constant of primitive unit cell, (a); bond length between adjacent atoms, (d); bond angle, (θ); donated electron by per Ca/B, (ρ); cohesive energy per atom in the unit cell, (E_c); energy band gap calculated within GGA-PBE, (E^{PBE}); energy band gap calculated within GGA-PBE+HSE06, ($E^{PBE+HSE}$); experimentally observed band gap, (E^{exp}) work function, (Φ); in-plane stiffness, (C); Poisson ratio, (ν); Raman active modes.

	a (Å)	d (Å)	θ (°)	ρ (e^-)	E_c (eV/$_{atom}$)	E^{PBE} (eV)	$E^{PBE+HSE}$ (eV)	E^{exp} (eV)	Φ (eV)	C (N/m)	ν	R-active modes (cm^{-1})
1T-CaF_2	3.58	2.29	76.88	1.64	5.42	7.17	9.49	-	8.67	44	0.24	281, 292, 299, 372
h-BN	2.51[31]	1.45	120	2.13	7.01[62]	4.65	5.77	5.5[63]	5.62	273[64]	0.22[64]	1365

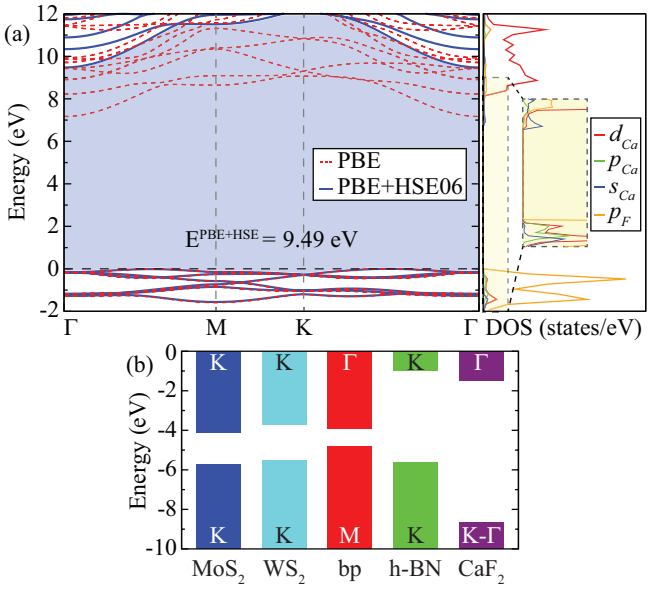

Fig. 2 (a)Electronic band structure and PDOS of 1T-CaF_2, (b) comparative band alignment of MoS_2, h-BN, black phosphorous (bp), WS_2, and 1T-CaF_2 where vacuum energies are set to zero.

and Ca-d orbitals, respectively. However, near conduction band minimum, the Ca-s orbitals exhibit higher density. In addition to GGA-PBE calculations, GGA-PBA + HSE06 functional is used in order to increase the accuracy of the electronic band calculations. As result monolayer CaF_2 retains its insulating behavior. PBE+HSE bands around Fermi level completely match the PBE bands however, PBE+HSE and PBE bands near conduction band do not match. Band gap of the 2D insulator widens to 9.49 eV. Wide band gap of 1T-CaF_2 is estimated to be higher than well-known insulator h-BN with band gap about ≈5.5 eV,[63] which makes 1T-CaF_2 an appealing insulator.

Band alignment comparison is an important method that is used to predict band modification in a heterostructure in various studies.[65–69] There are three types of heterojunctions; type I (straddling gap), type II (staggered gap), and type III (broken gap) heterojunction.[70] Band alignment of 1T-CaF_2 is compared with well-known monolayers such as semiconducting MoS_2, black phosphorous (bp), WS_2, and insulating h-BN by setting their vacuum energies to zero, presented in the Figure 2 (b). Valence band maximum (VBM) and conduction band minimum (CBM) are shown in the corresponding bars. 1T-CaF_2 has high lattice mismatch value with the given crystals. However, band gap alignment gives information about which type of heterojunction 1T-CaF_2 can form. In case of a heterostructure of 1T-CaF_2 and a semiconducting material such as MoS_2, black phosphorous, or WS_2 with suitable lattice constant, type I heterojunction is predicted to be formed. Contrarily, in case of a heterostructure of 1T-CaF_2 and h-BN like crystal with suitable lattice constant, type II heterojunction is predicted to be formed. Thus, stable ultra-thin CaF_2 with its wide electronic band gap is a suitable material for nanoscale heterojunction and substrate applications.

4 Nanoribbons of CaF_2: Width-Independent Band Gap

Nanoribbons of 2D materials have been drawing attention due to the unique properties and potential nanoscale applications they present.[71] In this section, nanoribbons (NRs) of CaF_2 are studied. Depending on the edge orientation of CaF_2 NRs, two different types are investigated, zigzag NRs and armchair NRs. An illustration of the NR structure is given in Figure 3a. The width of the NRs is indicated by the number N of Ca atoms in the unit cell. Note that for both types of NRs, the ratio between Ca and F atoms is stoichiometric, i.e., there are N Ca atoms and $2N$ F atoms in the unit cell. To study the width dependence of the electronic structure, for zigzag NRs,the NR width ranging from 4 to 10 and for armchair NRs, the NR width ranging from 5 to 15 are considered. It is found that for both type of NRs, there is no remarkable structural reconstruction, and the 1T structure is well maintained, as shown in Figure 3a. The edge energy of different NRs is shown in Figure 3b. For a NR with width N, the edge energy is defined as $(E_{NR} - NE_{2D})/(2L)$, where E_{NR} is the total energy of the NR unit cell, E_{2D} is the total energy of the unit cell of monolayer CaF_2, and L is the lattice constant of the NR. It describes how much extra energy is needed to create a new edge from the 2D layer. According to Figure 3b, for both zigzag and armchair NRs, the edge energy decreases as the width increases. Moreover, it is seen that the edge energy of zigzag CaF_2 NRs is smaller than that of armchair CaF_2 NRs when their widths are comparable (e.g., N=6 for zigzag NR and N=10 for armchair NR). A possible origin is that there are more dangling bonds at the armchair edge than at the zigzag edge. Overall, the magnitude of the edge energy is 0.2-0.4 eV/Å. In contrast, for NRs of typical transition-metal dichalcogenides like MoS_2 and WS_2, the edge energy is about 0.6 eV/Å[72]. Thus, the formation of CaF_2 NRs is relatively easier.

Next, the electronic properties of the NRs in terms of their width-dependent electronic band structures are investigated. Due to the quantum confinement effect, usually the band gap of a NR is larger than that in a 2D layer, and decreases as the width increases. In Figure 4a the band gap of different CaF_2 NRs is presented. It is interesting to see that the band gap is smaller than

View Article Online
DOI: 10.1039/C9CP06015D

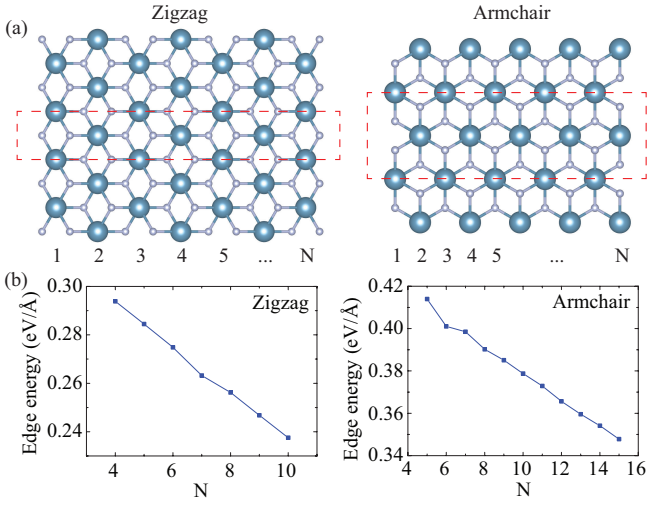

Fig. 3 (a) Structure of zigzag and armchair CaF_2 NRs. The dashed lines indicate the unit cells. (b) Edge energy of the NRs as a function of ribbon width.

the monolayer, and almost independent to the ribbon width. For zigzag NRs, the band gap is about 6.5 eV, and for armchair NRs, the gap is about 6.3 eV. In Figure 4b-c the band structures of selected NRs are given. For zigzag NRs, the CBM is located at the Γ point, whereas the VBM is at $\sim 2/3$ between Γ and X. On the other hand, both CBM and VBM are at the Γ point for armchair NRs. To further understand the width-independent band gap, one can analyze the character of the VBM and CBM states, as shown in Figure 4d. It appears that, all these states are mainly localized at the edge of the NRs, indicating strong edge effects in CaF_2 NRs. Because of the highly localized character, the transverse confinement effect to the CBM and VBM is quite small, leading to the width-independent band gap. Although the band gap is insensitive to the NR width, it can be more sensitive to the number of layers because the edge states can be affected by the out-of-plane confinement.

5 Conclusions

In this study, investigation on 1T-CaF_2 and its nanoribbons are carried out. Structural, vibrational, electronic properties are presented. Vibrational calculations revealed that monolayer CaF_2 has four Raman active modes. Having lower frequency phonon bands compare to h-BN revealed that 1T-CaF_2 is relatively softer material. In spite of having softer structure than h-BN, it is predicted to possess wider band gap of 7.17 eV by PBE and 9.49 eV by PBE+HSE06 functionals. Additionally, work function of 1T-CaF_2 is calculated to be much higher than h-BN while having lower cohesion between atoms in the unit cell by 1.58 eV/atom. In addition to the 2D structure of 1T-CaF_2, nanoribbons of CaF_2 are studied. Both in zigzag NRs and armchair NRs of CaF_2, 1T structure is maintained without reconstructions. Width dependent edge energy calculations revealed that edge energy decreases in both zigzag and armchair NRs with increasing width. With comparable widths, zigzag NRs of CaF_2 are found to have less edge energy than armchair NRs of CaF_2. Calculated edge energy showed that formation of CaF_2 NRs is easier compared to typical TMDs. In

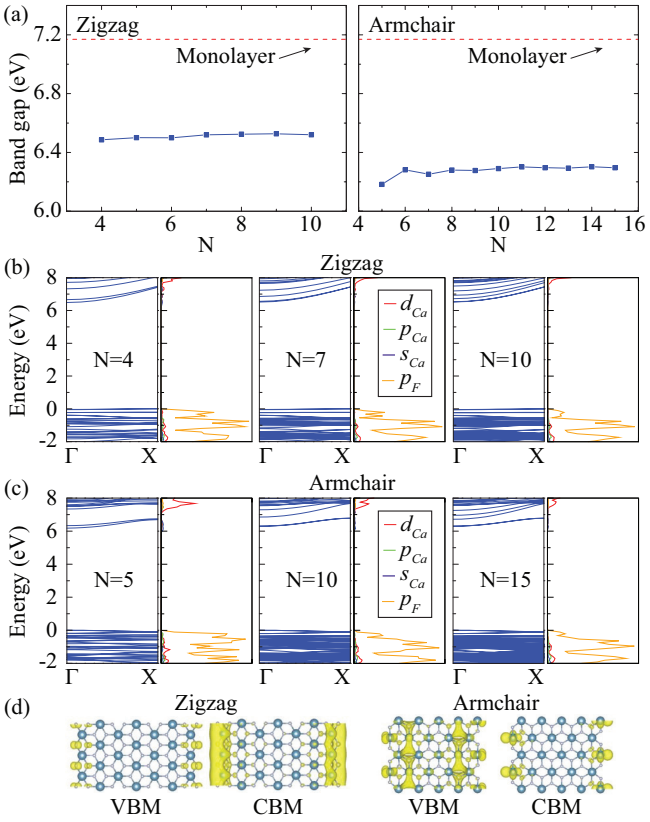

Fig. 4 (a) Band gap of the NRs as a function of ribbon width. (b) Band structure and PDOS of selected zigzag NRs. (c) Band structure and PDOS of selected armchair NRs. (d) The CBM and VBM states for the 7-zigzag NR and the 10-armchair NR.

the electronic band structures of NRs, band gap of NRs is found almost-independent to the width, and interestingly smaller than the monolayer CaF_2. Band decomposed charge densities of valence and conduction bands are examined and it is seen that states are localized at the edges of NRs. In conclusion, 1T-CaF_2 shows great potential in nanoelectronic applications in 2D and 1D form as a wide band gap insulator.

Conflicts of interest

There are no conflicts to declare.

Acknowledgements

Computational resources were provided by TUBITAK ULAKBIM, High Performance and Grid Computing Center (TR-Grid e-Infrastructure). H.S. Acknowledges financial support from the TUBITAK under the project number 117F095. H.S. acknowledges support from Turkish Academy of Sciences under the GEBIP program.

Notes and references

1 L. Sun and L. C. Chow, *Dent. Mater.*, 2008, **24**, 111–116.
2 H. H. Xu, J. L. Moreau, L. Sun and L. C. Chow, *Biomaterials*, 2008, **29**, 4261–4267.
3 D. S. Brauer, N. Karpukhina, R. V. Law and R. G. Hill, *J. Mater. Chem.*, 2009, **19**, 5629–5636.

View Article Online
DOI: 10.1039/C9CP06015D

4 A. Al-Noaman, S. C. Rawlinson and R. G. Hill, *J. Non-Cryst. Solids*, 2012, **358**, 1850–1858.

5 H. Yang, S. Yang, J. Kong, A. Dong and S. Yu, *Nat. Protoc.*, 2015, **10**, 382.

6 R. Adato and H. Altug, *Nat. Commun.*, 2013, **4**, 2154.

7 C. Lecaplain, C. Javerzac-Galy, M. Gorodetsky and T. Kippenberg, *Nat. Commun.*, 2016, **7**, 13383.

8 A. Lucca, M. Jacquemet, F. Druon, F. Balembois, P. Georges, P. Camy, J.-L. Doualan and R. Moncorgé, *Opt. Lett.*, 2004, **29**, 1879–1881.

9 A. Lucca, G. Debourg, M. Jacquemet, F. Druon, F. Balembois, P. Georges, P. Camy, J.-L. Doualan and R. Moncorgé, *Opt. Lett.*, 2004, **29**, 2767–2769.

10 M. Siebold, S. Bock, U. Schramm, B. Xu, J.-L. Doualan, P. Camy and R. Moncorgé, *Appl. Phys. B*, 2009, **97**, 327–338.

11 P. Aubry, A. Bensalah, P. Gredin, G. Patriarche, D. Vivien and M. Mortier, *Opt. Mater.*, 2009, **31**, 750–753.

12 M. S. Akchurin, T. T. Basiev, A. A. Demidenko, M. E. Doroshenko, P. P. Fedorov, E. A. Garibin, P. E. Gusev, S. V. Kuznetsov, M. A. Krutov, I. A. Mironov and V. V. Osiko, *Opt. Mater.*, 2013, **35**, 444–450.

13 S. E. Hatch, W. F. Parsons and R. J. Weagley, *Appl. Phys. Lett.*, 1964, **5**, 153–154.

14 T. P. Smith III, J. M. Phillips, W. M. Augustyniak and P. J. Stiles, *Appl. Phys. Lett.*, 1984, **45**, 907–909.

15 K. S. Novoselov, A. K. Geim, S. V. Morozov, D. Jiang, Y. Zhang, S. V. Dubonos, I. V. Grigorieva and A. A. Firsov, *Science*, 2004, **306**, 666–669.

16 K. S. Novoselov and A. K. Geim, *Nat. Mater.*, 2007, **6**, 183–191.

17 A. H. C. Neto, F. Guinea, N. M. R. Peres, K. S. Novoselov and A. K. Geim, *Rev. Mod. Phys.*, 2009, **81**, 109.

18 Q. H. Wang, K. Kalantar-Zadeh, A. Kis, J. N. Coleman and M. S. Strano, *Nat. Nanotechnol.*, 2012, **7**, 699.

19 M. Chhowalla, H. S. Shin, G. Eda, L.-J. Li, K. P. Loh and H. Zhang, *Nat. Chem.*, 2013, **5**, 263.

20 A. Ramasubramaniam, *Phys. Rev. B*, 2012, **86**, 115409.

21 K. F. Mak, C. Lee, J. Hone, J. Shan and T. F. Heinz, *Phys. Rev. Lett.*, 2010, **105**, 136805.

22 B. Radisavljevic, A. Radenovic, J. Brivio, V. Giacometti and A. Kis, *Nat. Nanotechnol.*, 2011, **6**, 147.

23 S. Tongay, J. Zhou, C. Ataca, K. Lo, T. S. Matthews, J. Li, J. C. Grossman and J. Wu, *Nano Lett.*, 2012, **12**, 5576–5580.

24 T. Georgiou, R. Jalil, B. D. Belle, L. Britnell, R. V. Gorbachev, S. V. Morozov, Y.-J. Kim, A. Gholinia, S. J. Haigh, O. Makarovsky, L. Eaves, L. A. Ponomarenko, A. K. Geim, K. S. Novoselov and A. Mishchenko, *Nat. Nanotechnol.*, 2013, **8**, 100.

25 H. Fang, S. Chuang, T. C. Chang, K. Takei, T. Takahashi and A. Javey, *Nano Lett.*, 2012, **12**, 3788–3792.

26 J. S. Ross, P. Klement, A. M. Jones, N. J. Ghimire, J. Yan, D. G. Mandrus, T. Taniguchi, K. Watanabe, K. Kitamura, W. Yao, D. H. Cobden and X. Xu, *Nat. Nanotechnol.*, 2014, **9**, 268.

27 S. Tongay, H. Sahin, C. Ko, A. Luce, W. Fan, K. Liu, J. Zhou, Y.-S. Huang, C.-H. Ho, J. Yan, D. F. Ogletree, S. Aloni, J. Ji, S. Li, J. Li, F. M. Peeters and J. Wu, *Nat. Commun.*, 2014, **5**, 3252.

28 A. Kuc, N. Zibouche and T. Heine, *Phys. Rev. B*, 2011, **83**, 245213.

29 I. Eren, F. Iyikanat and H. Sahin, *Phys. Chem. Chem. Phys.*, 2019, **21**, 16718–16725.

30 A. Molle, J. Goldberger, M. Houssa, Y. Xu, S.-C. Zhang and D. Akinwande, *Nat. Mater.*, 2017, **16**, 163.

31 H. Sahin, S. Cahangirov, M. Topsakal, E. Bekaroglu, E. Akturk, R. T. Senger and S. Ciraci, *Phys. Rev. B*, 2009, **80**, 155453.

32 L. Matthes, O. Pulci and F. Bechstedt, *New J. Phys.*, 2014, **16**, 105007.

33 P. Vogt, P. De Padova, C. Quaresima, J. Avila, E. Frantzeskakis, M. C. Asensio, A. Resta, B. Ealet and G. Le Lay, *Phys. Rev. Lett.*, 2012, **108**, 155501.

34 M. Dávila, L. Xian, S. Cahangirov, A. Rubio and G. Le Lay, *New J. Phys.*, 2014, **16**, 095002.

35 F.-f. Zhu, W.-j. Chen, Y. Xu, C.-l. Gao, D.-d. Guan, C.-h. Liu, D. Qian, S.-C. Zhang and J.-f. Jia, *Nat. Mater.*, 2015, **14**, 1020.

36 B. Cai, S. Zhang, Z. Hu, Y. Hu, Y. Zou and H. Zeng, *Phys. Chem. Chem. Phys.*, 2015, **17**, 12634–12638.

37 X.-L. Yu, L. Huang and J. Wu, *Phys. Rev. B*, 2017, **95**, 125113.

38 H. Shu, Y. Wang and M. Sun, *Phys. Chem. Chem. Phys.*, 2019, **21**, 15760–15766.

39 Y. Luo, K. Ren, S. Wang, J.-P. Chou, J. Yu, Z. Sun and M. Sun, *J. Phys. Chem. C*, 2019, **123**, 22742–22751.

40 B. Huang, G. Clark, E. Navarro-Moratalla, D. R. Klein, R. Cheng, K. L. Seyler, D. Zhong, E. Schmidgall, M. A. McGuire, D. H. Cobden, W. Yao, D. Xiao, P. Jarillo-Herrero and X. Xu, *Nature*, 2017, **546**, 270.

41 M. A. McGuire, H. Dixit, V. R. Cooper and B. C. Sales, *Chem. Mater.*, 2015, **27**, 612–620.

42 W. Xing, Y. Chen, P. M. Odenthal, X. Zhang, W. Yuan, T. Su, Q. Song, T. Wang, J. Zhong, S. Jia, X. C. Xie, Y. Li and W. Han, *2D Mater.*, 2017, **4**, 024009.

43 C. Gong, L. Li, Z. Li, H. Ji, A. Stern, Y. Xia, T. Cao, W. Bao, C. Wang, Y. Wang, Z. Q. Qiu, R. J. Cava, S. G. Louie, J. Xia and X. Zhang, *Nature*, 2017, **546**, 265.

44 K. Watanabe, T. Taniguchi and H. Kanda, *Nat. Mater.*, 2004, **3**, 404.

45 H. Jeong, S. Bang, H. M. Oh, H. J. Jeong, S.-J. An, G. H. Han, H. Kim, K. K. Kim, J. C. Park, Y. H. Lee, G. Lerondel and M. S. Jeong, *ACS Nano*, 2015, **9**, 10032–10038.

46 M. P. Levendorf, C.-J. Kim, L. Brown, P. Y. Huang, R. W. Havener, D. A. Muller and J. Park, *Nature*, 2012, **488**, 627.

47 L. H. Li and Y. Chen, *Adv. Funct. Mater.*, 2016, **26**, 2594–2608.

48 S. Ahn, G. Kim, P. K. Nayak, S. I. Yoon, H. Lim, H.-J. Shin and H. S. Shin, *ACS Nano*, 2016, **10**, 8973–8979.

49 L. Schowalter, R. Fathauer, R. Goehner, L. Turner, R. DeBlois, S. Hashimoto, J.-L. Peng, W. Gibson and J. Krusius, *J. Appl. Phys.*, 1985, **58**, 302–308.

50 Y. Y. Illarionov, A. G. Banshchikov, D. K. Polyushkin, S. Wachter, T. Knobloch, M. Thesberg, L. Mennel, M. Paur,

View Article Online
DOI: 10.1039/C9CP06015D

M. Stöger-Pollach, A. Steiger-Thirsfeld, M. I. Vexler, M. Waltl, N. S. Sokolov, T. Mueller and T. Grasser, *Nat. Electron.*, 2019, 1.

51 G. Kresse and J. Hafner, *Phys. Rev. B*, 1993, **47**, 558–561.

52 G. Kresse and J. Furthmüller, *Phys. Rev. B*, 1996, **54**, 11169–11186.

53 P. E. Blöchl, *Phys. Rev. B*, 1994, **50**, 17953.

54 J. P. Perdew, K. Burke and M. Ernzerhof, *Phys. Rev. Lett.*, 1996, **77**, 3865–3868.

55 S. Grimme, *J. Comput. Chem.*, 2006, **27**, 1787–1799.

56 J. Heyd, G. E. Scuseria and M. Ernzerhof, *J. Chem. Phys.*, 2003, **118**, 8207–8215.

57 A. V. Krukau, O. A. Vydrov, A. F. Izmaylov and G. E. Scuseria, *J. Chem. Phys.*, 2006, **125**, 224106.

58 D. Alfe, *Comput. Phys. Commun.*, 2009, **180**, 2622–2633.

59 G. Henkelman, A. Arnaldsson and H. Jónsson, *Comput. Mater. Sci.*, 2006, **36**, 354–360.

60 C. Ataca, M. Topsakal, E. Akturk and S. Ciraci, *J. Phys. Chem. C*, 2011, **115**, 16354–16361.

61 H. Sahin, S. Cahangirov, M. Topsakal, E. Bekaroglu, E. Akturk, R. T. Senger and S. Ciraci, *Phys. Rev. B*, 2009, **80**, 155453.

62 A. Janotti, S.-H. Wei and D. J. Singh, *Phys. Rev. B*, 2001, **64**, 174107.

63 J. A. Carlisle, E. L. Shirley, L. J. Terminello, J. J. Jia, T. A. Callcott, D. L. Ederer, R. C. C. Perera and F. J. Himpsel, *Phys. Rev. B*, 1999, **59**, 7433–7445.

64 M. Yagmurcukardes, C. Bacaksiz, E. Unsal, B. Akbali, R. Senger and H. Sahin, *Phys. Rev. B*, 2018, **97**, 115427.

65 D. O. Scanlon, C. W. Dunnill, J. Buckeridge, S. A. Shevlin, A. J. Logsdail, S. M. Woodley, C. R. A. Catlow, M. J. Powell, R. G. Palgrave, I. P. Parkin, G. W. Watson, T. W. Keal, P. Sherwood, A. Walsh and A. A. Sokol, *Nat. Mater.*, 2013, **12**, 798.

66 V. O. Özcelik, J. G. Azadani, C. Yang, S. J. Koester and T. Low, *Phys. Rev. B*, 2016, **94**, 035125.

67 M. Yagmurcukardes, E. Torun, R. T. Senger, F. M. Peeters and H. Sahin, *Phys. Rev. B*, 2016, **94**, 195403.

68 Z. Kahraman, A. Kandemir, M. Yagmurcukardes and H. Sahin, *J. Phys. Chem. C*, 2019, **123**, 4549–4557.

69 M. Yagmurcukardes, S. Ozen, F. Iyikanat, F. Peeters and H. Sahin, *Phys. Rev. B*, 2019, **99**, 205405.

70 T. Ihn, *Semiconductor Nanostructures: Quantum States and Electronic Transport*, Oxford University Press, 2010.

71 M. Yagmurcukardes, F. M. Peeters, R. T. Senger and H. Sahin, *Appl. Phys. Rev.*, 2016, **3**, 041302.

72 F. Güller, A. M. Llois, J. Goniakowski and C. Noguera, *Phys. Rev. B*, 2015, **91**, 075407.